ACS APPLIED MATERIALS & INTERFACES

Research Article

www.acsami.org

Gold Nanorod Enhanced Two-Photon Excitation Fluorescence of Photosensitizers for Two-Photon Imaging and Photodynamic Therapy

Tingting Zhao,[†,‡] Kuai Yu,[†,‡,§] Lin Li,[‡] Taishi Zhang,[§] Zhenping Guan,[‡] Nengyue Gao,[‡] Peiyan Yuan,[‡] Shuang Li,[‡] Shao Qin Yao,[‡] Qing-Hua Xu,*[,‡,§] and Guo Qin Xu*[,‡]

[‡]Department of Chemistry, National University of Singapore, 3 Science Drive 3, Singapore 117543

[§]NUS Graduate School for Integrative Sciences and Engineering, National University of Singapore, Singapore 117456

Supporting Information

ABSTRACT: Plasmon enhancement of optical properties is both fundamentally important and appealing for many biological and photonic applications. Although metal-enhanced two-photon excitation fluorescence has been demonstrated in the solid substrates, there is no report on metal enhanced overall two-photon excitation fluorescence in the colloid system. Here we systematically investigated gold nanorod enhanced one- and two-photon excitation fluorescence of a porphyrin molecule, T790. The separation distance between the metal core and T790 was varied by adjusting the silica shell thickness from 13 to 42 nm. One- and two-photon excitation fluorescence intensities of T790 were found to strongly depend on the thickness of silica shell that separates gold nanorod and T790. The optimum one- and two-photon excitation fluorescence enhancement was found to occur at shell thicknesses of 34 and 20 nm, with enhancement factors of 2.1 and 11.8, respectively. Fluorescence lifetime of T790 steadily decreased as the shell thickness decreased. The observed two-photon excitation fluorescence enhancement is ascribed to a combination effect of local electric field amplification and competition between increased radiative and non-radiative decay rates. Core-shell nanoparticles that displayed enhanced two-photon excitation fluorescence were also found to exhibit significantly improved singlet oxygen generation capability under two-photon excitation. The applications of these nanoparticles as effective agents for two-photon cell imaging and nano-photosensitizers for two-photon photodynamic therapy with improved efficiency have also been demonstrated in HepG2 cancer cells. The combined advantages of enhanced two-photon excitation fluorescence and two-photon induced singlet oxygen generation make these core-shell nanoparticles as attractive agents for two-photon imaging guided two-photon photodynamic therapy.

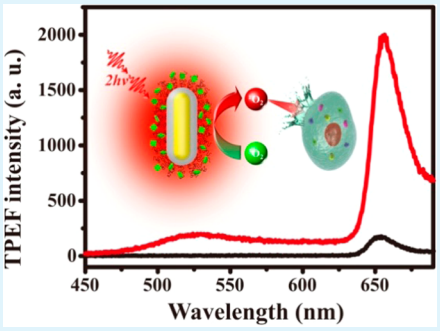

KEYWORDS: *gold nanorods, core−shell nanoparticles, plasmon resonance enhancement, nano-photosensitizers, two-photon imaging, two-photon photodynamic therapy*

INTRODUCTION

Metal nanoparticles, such as silver (Ag) and gold (Au), are known to display many unique optical properties such as Plasmon resonance.[1,2] Plasmon resonance arises from collective oscillation of conduction band electrons of metal surfaces or metal nanoparticles. Plasmon resonance can induce enhanced local electromagnetic fields and modulate optical properties of nearby chromophores. These appealing characters make metal nanoparticles attractive in many applications such as surface-enhanced Raman spectroscopy,[3,4] metal-enhanced fluorescence,[5−9] and metal enhanced nonlinear optical responses.[10−12]

Most of the previous studies on metal-enhanced fluorescence are focused on enhancing the conventional one-photon excitation fluorescence and their applications.[13−17] Multi-photon excitation fluorescence is expected to display much larger signal enhancement since it is proportional to a higher order function of local electric field. Kano et al. showed that two-photon excitation of an organic dye was affected by field-enhancing factors of 270 for silver films and 80 for gold films.[18] Wenseleers et al. reported five orders of magnitude enhancement of two-photon absorption for dyes on silver nanoparticle fractal clusters in films using two-photon fluorescence microscopy measurements.[19] Jung et al. recently demonstrated that two-photon excitation fluorescence of fluorophores on Au patterned surface was enhanced by ∼100 times compared with the molecules on the glass surface, which allowed enhanced sensitivity for DNA detection.[20] However, previous studies on plasmon enhanced two-photon excitation fluorescence were usually conducted on the solid substrates[18−21] and very few studies had been reported on the colloid-based systems because of the difficulty in preparing highly reproducible nanostructures and controlling the fluorophores around metal nanoparticles. Furthermore, studies in films are generally complicated by the plasmon coupling between neighboring nanoparticles. A few

Received: November 19, 2013
Accepted: February 3, 2014
Published: February 3, 2014

available reports on colloid-based systems focus on plasmon enhanced two-photon absorption. Hernandez et al. reported a 157-fold enhancement of two-photon absorption of the chromophores using salt-aggregated spherical gold nanoparticles by using z-scan techniques.[22] A very recent report by Sivapalan et al. indicated that the two-photon absorption of an organic dye was enhanced by ~40 times by the unaggregated gold nanorods in colloid suspensions.[23] In addition to the discrepancy in enhancement factors of two-photon absorption, so far there was no report of enhanced overall two-photon excitation fluorescence (i.e., two-photon action cross section, the product of two-photon absorption efficiency and emission quantum yield) in colloid-based systems. Two-photon action cross section, rather than two-photon absorption itself, is the performance indicator of materials for applications in two-photon imaging. A major difficulty in achieving enhanced overall two-photon excitation fluorescence is that enhanced two-photon excitation efficiency is generally accompanied by fluorescence quenching (decreased quantum yield). Both two-photon excitation efficiency and fluorescence quantum yield are strongly dependent on the separation distance between the chromophores and metal core.[13,23−26] A systematical investigation of separation distance dependent plasmon resonance effect on two-photon excitation fluorescence will help to achieve an overall enhancement in two-photon excitation fluorescence.

Gold nanorods (Au NRs) are notable for large two-photon action cross section,[27] tunable longitudinal plasmon band, large-scale preparation, biocompatibility, and chemical inertness, which make them extensively exploited for applications in biomedical sensing,[28−30] two-photon imaging,[31,32] gene and drug delivery,[33,34] photo-thermal and photodynamic therapy.[35−37] Au NRs have been utilized to investigate fluorescence enhancement at single particle level,[38,39] in colloid,[40,41] and in the embedded film.[42] Compared with traditional one-photon fluorescence (OPEF), two-photon excitation fluorescence (TPEF) has various advantages. First, TPEF emission of fluorophores is easy to be separated from the excitation light owing to the large effective anti-Stokes shift. In addition, TPEF uses near-infrared light as excitation source, which suffers less scattering and allows deep penetration into biological tissues. Most importantly, two-photon excitation rate is proportional to the fourth power of electric field, which allows three-dimensional confined excitation and can be dramatically enhanced by the amplified local electric field of plasmon resonance. It is attractive to develop Au NR-fluorophore composite nanostructures for various two-photon excitation based applications.

In this work, we conducted a systematic investigation of distance dependent one- and two-photon excitation fluorescence enhancement in a core-shell nanostructure consisting of an Au NR core, a silica shell with controllable thickness, and a layer of porphyrin molecules. The composite nanoparticles were prepared by covalently binding porphyrin molecules (T790) with amino group modified silica coated Au NRs via formation of a stable amide bond. The silica shell acted as a spacer to control the distance between Au NR and T790. One- and two-photon excitation fluorescence of these core-shell nanoparticles were optimized by adjusting the silica shell thickness from 13 to 42 nm. The fluorescence lifetime measurements have been conducted to understand the enhancement mechanisms. Singlet oxygen generation capability of these core−shell nanoparticles under two-photon excitation has been evaluated in HepG2 cells. Two-photon imaging and two-photon photodynamic activity of these AuNR/SiO_2-T790 nanoparticles on cancer cells have also been demonstrated.

EXPERIMENTAL SECTION

Materials and Methods. Cetyltrimethylammonium bromide (CTAB) and ascorbic acid were purchased from Alfa Aesar. Tetraethoxysilane (TEOS), silver nitrate ($AgNO_3$), sodium borohydride ($NaBH_4$), hydrogen tetrachloroaurate (III) hydrate ($HAuCl_4 \cdot 3H_2O$), N-(3-dimethyl-aminopropyl)-N′-ethylcarbodiimide hydrochloride (EDC), N-hydroxysuccinimide (NHS), 3-aminopropyltrimethoxysilane (APTEOS), trimethoxyl(octadecyl)silane (OTMS), meso-tetra(4-carboxyphenyl) porphyrin (T790), and aqueous ammonia (25%) were purchased from Sigma Aldrich. All solvents are analytical grade and used as-received without further purification.

Transmission electron microscopic (TEM) images were taken on a JEOL 2010 microscope operating at an acceleration voltage of 200 kV. UV−vis absorption/extinction and fluorescence spectra were measured using a Shimadzu UV 2550 Spectrometer and a Horiba JobinYvon FluoroMax-4 Spectrofluorometer, respectively. The fluorescence lifetimes were measured by using a time-correlated single-photon counting (TCSPC) technique. The frequency-doubled output (420 nm) of an Avesta TiF-100M femtosecond Ti:sapphire oscillator was used as the excitation source. Fluorescence at 650 nm was collected by an optical fiber that is directed to an avalanche photodiode (APD). The signals were processed by a TCSPC module (PicoQuant, PicoHarp 300) with temporal resolution of ~150 ps.

Preparation of Au NRs. Au NRs were prepared according to a previously reported method.[43−45] CTAB aqueous solution (0.1 M, 10 mL) was mixed with $HAuCl_4$ (50 mM, 50 μL) and ice-cold $NaBH_4$ (10 mM, 0.6 mL) to form a brownish-yellow seed solution. This seed solution was kept at room temperature for at least 2 h. The growth solution is a mixture of CTAB solution (0.1 M, 40 mL), $HAuCl_4$ (50 mM, 0.4 mL), different amount of $AgNO_3$ (10 mM, 0.34 mL), HCl (1 M, 0.8 mL) and ascorbic acid (0.1 M, 0.32 mL). The growth solution became colourless after gentle mixing. The gold seed solution (100 μL) was then added into the growth solution and the reaction mixture was left undisturbed overnight. The obtained Au NRs were purified once by washing with deionized water to remove excess CTAB and re-dispersed in 40 mL of de-ionized water.

Preparation of Silica-Coated Au NRs (AuNR/SiO_2). Ten milliliters of Au NR solution was centrifuged and redispersed in 10 mL of deionized water. One hundred microliters of 0.1 M NaOH solution was added under stirring. Different amounts of pure TEOS were subsequently injected three times under stirring at 30 min intervals. A silica layer was formed on the surface of Au NR through hydrolysis and condensation of TEOS after a few hours. The obtained AuNR/SiO_2 nanoparticles were isolated by centrifugation, washed with deionized water several times, and then dispersed in deionized water for further use.

Preparation of T790-Doped Silica-Coated Au NRs (AuNR/SiO_2-T790). Silica coated Au NRs were first functionalized with long hydrophobic alkyl chains and amino groups using OTMS and APTEOS. 10 mL of AuNR/SiO_2 in ethanol solution was first added into 100 μL of ammonium hydroxide (25%) and stirred for 5 min before 100 μL of OTMS in chloroform solution (2.5%) was added. After stirring the mixture for another 7 h, 100 μL of APTEOS in chloroform solution (25%) was added. The mixture reacted overnight at room temperature to afford the amino group functionalized AuNR/SiO_2.

AuNR/SiO_2-T790 nanoparticles were prepared by coupling amino group functionalized AuNR/SiO_2 nanoparticles with T790. 5 μL of 0.1 M NHS, 5 μL of 0.1 M EDC, and 0.5 mL of 1.0 mM T790 was first dissolved in 4.0 mL of DMF. After vigorous stirring for 30 min, 1.0 mL of prepared amino group functionalized AuNR/SiO_2 nanoparticles were added into the mixture. The reaction was allowed to further proceed for 10 h and AuNR/SiO_2-T790 nanoparticles were collected by centrifugation. Excess T790 molecules were removed by centrifuging and washing the nanoparticles with DMF several times.

The obtained nanoparticles were then dispersed in DMF or aqueous medium for various optical characterizations and cell experiments.

Preparation of SiO_2-T790 Nanoparticles. Silica nanoparticles were prepared according to the Stöber method.[46] Aqueous ammonia (25%, 3.0 mL), pure TEOS (1.5 mL) were added into 50 mL of ethanol solution. The mixture reacted overnight at room temperature. SiO_2-T790 nanoparticles were prepared by replacing Au NR core with a silica nanosphere. The prepared SiO_2-T790 nanoparticles are quite monodisperse with an averaged diameter of ~100 nm (see Figure S1 in the Supporting Information).

Two-Photon Excitation Fluorescence Measurements. Two-photon excitation fluorescence (TPEF) measurements were performed by using a femtosecond Ti: sapphire oscillator (Avesta TiF-100M) with output laser pulses centered at 820 nm and average power of 100 mW as the excitation source. The laser pulses have pulse duration of 80 fs and repetition rate of 84.5 MHz. The laser beam was focused onto the sample that was contained in a cuvette with path length of 1.0 cm. The emission from the sample was collected at a 90° angle by a pair of lenses and an optical fiber that was connected to a monochromator (Acton, Spectra Pro 2300i) coupled CCD (Princeton Instruments, Pixis 100B) system. A shortpass filter with cut-off wavelength of 750 nm was placed before the monochromator to minimize the scattering from the pump beam.

Detection of Singlet Oxygen Generation. Singlet oxygen generation under one- and two-photon excitation were characterized by photo-oxidation of ABDA in DMF and aqueous solution. ABDA can react irreversibly with singlet oxygen, which causes a decrease in the ABDA absorption band at 377 nm. The solutions containing AuNR/SiO_2-T790 nanoparticles and ABDA were irradiated with band selected white light source at 420 ± 1 nm (one-photon excitation) or fs laser pulses at 800 nm (two-photon excitation) from a Ti:sapphire oscillator seeded regenerative amplifier (Spectra Physics Spitfire pro). Two-photon excitation singlet oxygen generation experiments were performed by using an unfocused laser beam with beam area of 0.3 cm^2 and pulse energy of 0.9 mJ, which gives a comparable power density to that of two-photon excitation fluorescence measurements. Absorbance of the solution at 377 nm was recorded at 1 min intervals using a UV−vis spectrometer. For direct comparison, the same experiments were performed on solution containing SiO_2-T790 nanoparticles and ABDA under the same condition.

Cell Culture. HepG2 cell line was chosen as the model system. The HepG2 cancer cells were incubated in Dulbecco's modified Eagle medium (DMEM) containing 10% fetal bovine serum, 100.0 mg/L streptomycin, and 100 IU/mL penicillin. Cells were maintained in a humidified atmosphere of 5% CO_2 at 37 °C.

Two-Photon Photodynamic Activity on Cancer Cells. HepG2 cancer cells were seeded on a 96 well plate and grown until 70−80% confluence, then treated with AuNR/SiO_2-T790 and SiO_2-T790 suspension for 3 h in DMEM, followed by changing with fresh DMEM media. Two-photon photodynamic therapy experiments were performed under the same experimental condition as the two-photon singlet oxygen generation experiments by using an unfocused femtosecond laser beam (0.3 cm^2) and pulse energy of 0.9 mJ at 800 nm as the illumination source. Cells were exposed to the femtosecond laser beam from 0 to 8 min irradiation period. The irradiated plates were sent back to the incubator overnight and cell viability was measured with the XTT assay.

Two-Photon Excitation Cell Imaging. HepG2 cancer cells were seeded on glass-bottom dishes and grown until 70−80% confluence. AuNR/SiO_2-T790 solution was added into the media and incubated for 3hrs. After washing with PBS buffer solution, fresh DMEM media were added. Two-photon imaging was conducted on a Leica TCS SP5 X confocal microscope using a femtosecond Ti-sapphire oscillator (820 nm) as the excitation source. Images were processed by using Leica Application Suite Advanced Fluorescence (LAS AF) software.

FDTD Simulation. The simulation was performed using Lumerical FDTD Solutions. The simulation region was a 2 μm × 2 μm × 2 μm cube with background refractive index of 1.43 to represent DMF solvent. In the center of the simulation region, an Au NR with dimensions of 23 × 81 nm^2 that gives a longitudinal SPR band maximum at 820 nm was chosen to mimic our experimental conditions. The permittivity of gold was taken from Johnson and Christy's data.[47] The whole Au NR was embedded in a 42 nm thick layer of silica with refractive index of 1.46. The Au NR-silica structure with its surrounding space was meshed at 0.7 nm. The incident light is polarized along the longitudinal direction of the Au NR with wavelength ranging from 400 to 1000 nm. Power monitors were set to obtain both the E field distribution as well as extinction. A series of power monitors was set at different distance to calculate the distance dependence of E-field.

RESULTS AND DISCUSSION

The preparation procedure of AuNR/SiO_2-T790 nanoparticles is illustrated in Scheme 1. Au NRs were prepared by using a seed-mediated, CTAB-assisted method.[43−45] AuNR/SiO_2-T790 nanoparticles were prepared by using a two-step sol-gel method.[48] The mixture of TEOS and Au NR solution reacted for different time periods to grow silica shell with various thicknesses on the surface of Au NRs. The surface of AuNR/SiO_2 was subsequently modified with long hydrophobic alkyl chains and amino groups using OTMS and APTEOS.[49] The use of APTEOS introduces amino groups onto the silica surface of AuNR/SiO_2, which offer bonding sites for fluorophores. Most cross-linker reagents have side reactions in the aqueous solution during the coupling process, which can be minimized by conducting the coupling reaction in DMF solution. Modification of long hydrophobic alkyl chains on the silica surface allows AuNR/SiO_2 to disperse well in DMF solution for further reactions.[49] T790 were covalently linked to the silica shell via formation of a stable amide bond using EDC and NHS.[50,51] Conjugation of T790 molecules to AuNR/SiO_2 nanoparticles was performed in DMF solution at room temperature overnight. The prepared AuNR/SiO_2-T790 nanoparticles are quite stable so that T790 molecules will not be released from nanoparticles after several months. This conjugation method allows incorporation of any amine-containing fluorophores into the silica shell to load a large amount of fluorophores or biomolecules.

Scheme 1. Schematic Procedure for Preparation of AuNR/SiO_2-T790 Nanoparticles

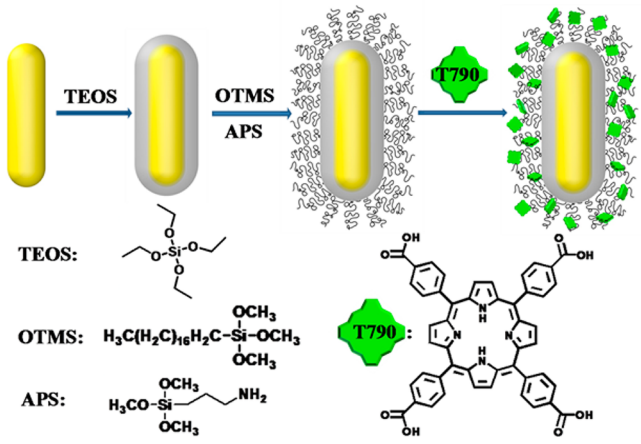

Figure 1 shows typical TEM images of Au NRs, AuNR/SiO_2, functionalized AuNR/SiO_2 and AuNR/SiO_2-T790 nanoparticles. The obtained Au NRs have an average length of 85 nm and width of 20 nm (Figure 1a) with an aspect ratio of 4.25. These Au NRs exhibit a longitudinal Plasmon band at 820 nm. The TEM image of AuNR/SiO_2 nanoparticles clearly shows

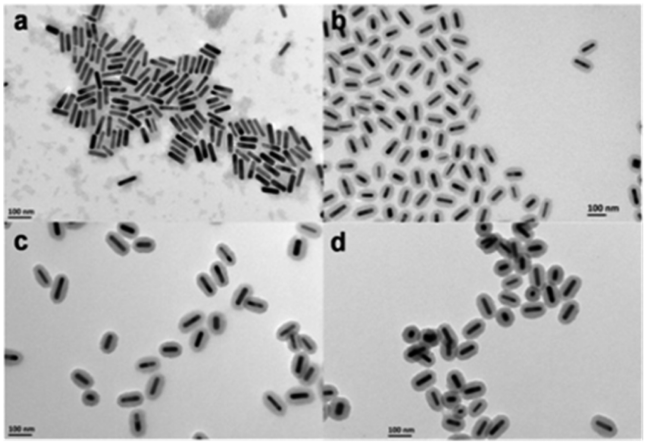

Figure 1. Typical TEM images of (a) Au NRs, (b) AuNR/SiO_2, (c) surface functionalized AuNR/SiO_2, and (d) AuNR/SiO_2(28 nm)-T790 nanoparticles.

that each particle consists of an Au NR core and a uniform silica shell (Figure 1b). The silica shell thickness remained nearly unchanged during the subsequent modification processes (Figure 1c, d). The thickness of silica shells can be determined from the utmost outside of the particle to the edge of Au NRs. Metal enhanced fluorescence has been known dependent on the metal-chromophore separation distance.[13,26,52] Silica shell acts as a spacer to separate Au NR and T790 and adjust their separation distance to achieve optimum enhancement. The surface of silica shell offers bonding sites for conjugation with a large amount of T790. After coating with silica and T790, the longitudinal SPR band of Au NRs slightly shifts to red owing to higher refractive index of silica than that of aqueous media.

Core-shell AuNR/SiO_2-T790 nanoparticles with silica shell thickness from 13 to 42 nm were prepared by changing TEOS amount and reaction time to investigate the distance-dependent fluorescence enhancement effects. Au NRs are known to display strong two-photon photoluminescence (TPPL),[53] which overwhelmed the two-photon excitation fluorescence of T790 in aqueous solution (see Figure S1 in the Supporting Information). Our recent studies showed that TPPL of Au NRs was strongly solvent dependent and TPPL intensity of Au NRs in DMF was quenched by ~91-fold compared to that in H_2O.[54] However, quantum yield of T790 was quenched by a less extent in DMF (see Figure S1 in the Supporting Information) compared to that in H_2O. To suppress the interference from the contribution of TPPL of Au NRs to TPEF of T790, the separation distance dependent plasmon enhancement effects were investigated in DMF solvent. Figure 2 shows the results of two typical AuNR/SiO_2-T790 nanoparticles with silica thickness of 20 and 34 nm. To quantitatively calculate the enhancement effect by Au NR in AuNR/SiO_2-T790, we used SiO_2-T790 nanoparticles in DMF solution as the control to ensure identical environment of T790 as in AuNR/SiO_2-T790 nanoparticles. The absorbance and fluorescence maxima of SiO_2-T790 in DMF solution remained at 419 and 651 nm, respectively (see Figure S2 in the Supporting Information), identical to those of T790 in DMF (Table 1).

Table 1. Optical Properties of T790 and SiO_2-T790 Nanoparticles

dye	solvent	$\lambda_{max,abs}$(nm)	$\lambda_{max,em}$(nm)	ϕ (%)[a]	δ (820 nm, GM)[a]
T790	DMF	419	650	~15[b]	~2[b]
SiO_2-T790	DMF	419	651	~14.9	~2

[a]Quantum yield and TPA cross-section at 820 nm: measured in DMF solutions. T790 in DMF solution was used as the standard for both quantum yield and TPA cross-section measurements. [b]Value taken from ref 55.

Figure 2a–c shows extinction, OPEF, and TPEF spectra of AuNR/SiO_2-T790 nanoparticles with silica shell thickness of 20 nm in DMF solutions. In addition to strong SPR bands of Au NRs at 510 and 820 nm, extinction spectrum of AuNR/SiO_2-T790 shows an extra absorption band peaking at 420 nm owing to absorption of T790 molecules. The amount of T790 molecules covalently linked to silica shell could be estimated

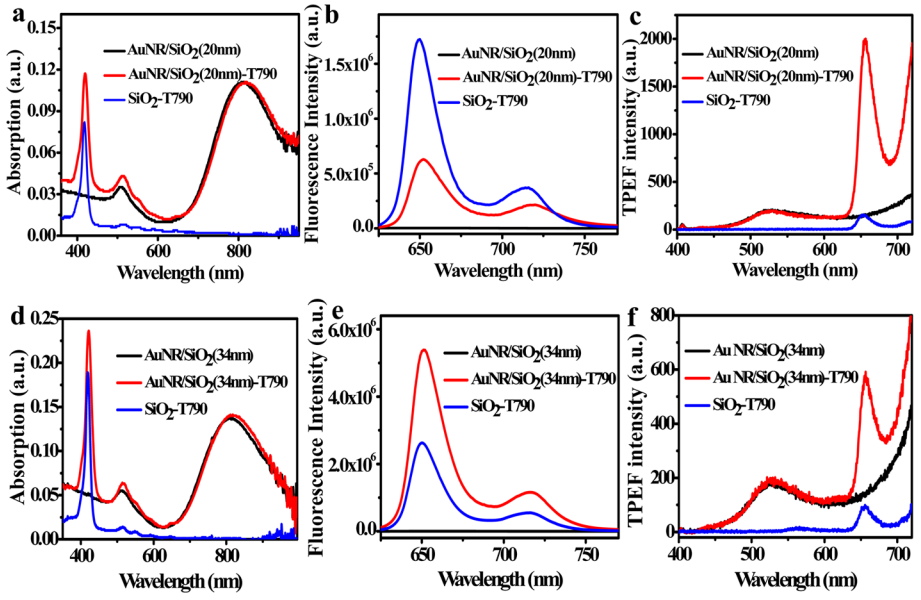

Figure 2. (a, d) Extinction spectra, (b, e) OPEF, and (c, f) TPEF spectra of SiO_2-T790, AuNR/SiO_2 and two typical AuNR/SiO_2-T790 nanoparticles with silica shell thickness of (a–c) 20 and (d–f) 34 nm in DMF solutions. [AuNR/SiO_2-T790] = 30 pM.

from the absorption/extinction spectra. The relative ratio of T790 to Au NR was determined by using $N_{T790}/N_{AuNR} = A_{T790}/\varepsilon_{T790}]/[A_{AuNR}/\varepsilon_{AuNR}]$, where A_{T790}, ε_{T790}, A_{AuNR}, and ε_{AuNR} are the absorbance/extinction and molar extinction coefficients of T790 at 420 nm and Au NRs at 820 nm respectively. $\varepsilon_{T790} = 3.44 \times 10^5\ M^{-1}\ cm^{-1}$ and $\varepsilon_{AuNR} = 5 \times 10^9\ M^{-1}\ cm^{-1}$.[56,57] It can be roughly estimated that each AuNR/SiO_2(20 nm)-T790 nanoparticle contains ~12500 T790 molecules. OPEF spectra of AuNR/SiO_2-T790 and SiO_2-T790 displayed similar spectra with two emission bands centered at 650 and 715 nm. However, fluorescence intensity of AuNR/SiO_2(20 nm)-T790 was quenched by ~2.8 times (equivalent to enhancement factor of 0.36) compared to that of SiO_2-T790 (Figure 2b). TPEF spectra of AuNR/SiO_2-T790 show very different behaviors. In addition to the emission band centered at 655 nm arising from T790, another broad emission band centered at 530 nm was also observed, which is due to TPPL of Au NRs as the same emission band was also observed in AuNR/SiO_2. TPPL intensities of Au NRs (530 nm band) in AuNR/SiO_2 and AuNR/SiO_2-T790 were nearly identical, indicating that the presence of T790 has little influence on TPPL of Au NRs. In contrast to the quenching effect in OPEF, TPEF intensity of T790 at 655 nm of AuNR/SiO_2(20 nm)-T790 was found to be enhanced by 11.8-fold relative to the SiO_2-T790 control sample (Figure 2c).

Another core-shell nanoparticle, AuNR/SiO_2(34 nm)-T790 that has a silica shell thickness of 34 nm, was found to display different enhancement factors: 2.1 and 4.0 for OPEF and TPEF compared to the corresponding control sample, respectively (Figure 2e&f). This is consistent with the previous results that metal enhanced/modulated fluorescence is strongly separation distance dependent.[13,24−26] To systematically study distance dependent enhancement effects, we have prepared a series of AuNR/SiO_2-T790 nanoparticles with silica shell thickness of 13, 20, 28, 34, and 42 nm by changing the TEOS amount and reaction time (Figure 3a-e). OPEF and TPEF enhancement factors of different AuNR/SiO_2-T790 nanoparticles in DMF solution are summarized in Figure 3f and Table 2. The optimum OPEF enhancement occurs at a shell thickness of 34 nm with enhancement factor of 2.1. Larger shell thickness results in reduced or nearly no fluorescence enhancement. Thinner shell thickness causes less fluorescence enhancement or even fluorescence quenching. TPEF displays similar dependence on silica shell thickness. The optimum TPEF enhancement occurs at a shell thickness of 20 nm with enhancement factor of 11.8. Deviation from this optimum shell thickness resulted in a decreased enhancement factor.

To understand the fluorescence enhancement mechanisms, we have measured fluorescence lifetimes of T790 in SiO_2-T790 and different AuNR/SiO_2-T790 nanoparticles (Figure 3g) by using time-correlated single photon counting (TCSPC) technique. The fluorescence decay of SiO_2-T790 can be well-fit with a single exponential decay with a lifetime of ~7.79 ns. The fluorescence lifetimes of AuNR/SiO_2-T790 in DMF solution were obtained to be 2.17, 3.25, 4.18, 5.16, and 7.75 ns for shell thickness of 13, 20, 28, 34, and 42 nm, respectively (Table 2). Fluorescence lifetimes of T790 in AuNR/SiO_2-T790 are shorter than that in SiO_2-T790 without a metal core and decrease gradually when silica shell thickness decreases.

In the presence of metal nanoparticles, three different metal-chromophore interactions will influence the fluorescence intensity of chromophores. First, local electric field amplification due to plasmon resonance will cause increased excitation

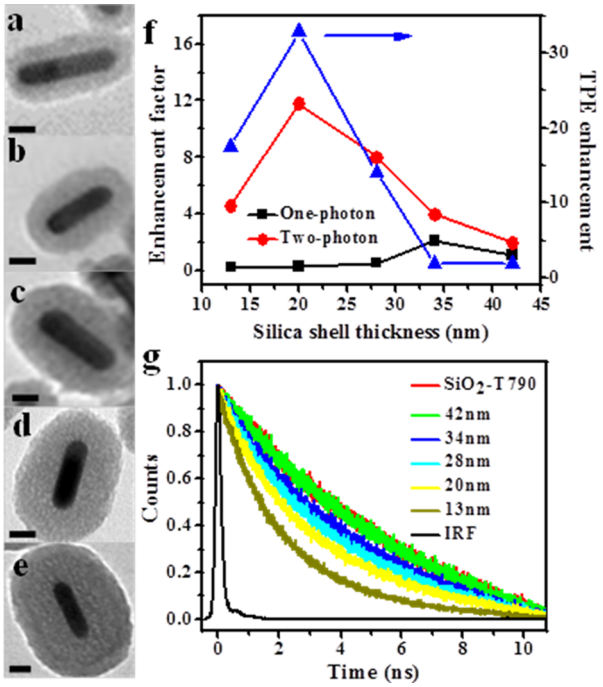

Figure 3. (a−e) TEM images, (f) one- and two-photon excitation fluorescence enhancement factors, and (g) fluorescence lifetime decay of AuNR/SiO_2-T790 with different silica shell thickness (13, 20, 28, 34, 42 nm) in DMF solutions (scale bar is 20 nm). The two-photon excitation (TPE) efficiency enhancement, estimated from the ratio of TPEF enhancement factor to quantum yield enhancement factor, is also plotted in f. IRF in g is the instrument response function.

Table 2. OPEF and TPEF Enhancement Factors and Fluorescence Lifetimes of SiO_2-T790 and AuNR/SiO_2-T790 with Different Silica Shell Thickness in DMF Solution

samples	silica shell thickness (nm)	OPEF enhancement factor	TPEF enhancement factor	fluorescence lifetime (ns)
AuNR/SiO_2-T790 (1)	13	0.26	4.6	2.17
AuNR/SiO_2-T790 (2)	20	0.36	11.8	3.25
AuNR/SiO_2-T790 (3)	28	0.54	8	4.18
AuNR/SiO_2-T790 (4)	34	2.1	4	5.16
AuNR/SiO_2-T790 (5)	42	1.1	2	7.75
SiO_2-T790				7.79

efficiency and consequently increased fluorescence intensity. The extent of enhancement depends on the overlap between excitation wavelength and Plasmon resonance. This enhancement effect does not change fluorescence lifetime of chromophores. The second factor is enhanced radiative decay rate, which causes increased fluorescence quantum yield and shortened fluorescence lifetime. This enhancement mechanism generally depends on spectral overlap between SPR band of metal nanoparticles and emission spectrum of chromophores. The third effect is energy transfer from the chromophore to metal nanoparticle, which generally quenches the fluorescence of chromophore and shortened its fluorescence lifetime. All three factors depend on the separation distance between the chromophore and metal nanoparticle, which result in strong

dx.doi.org/10.1021/am405214w | ACS Appl. Mater. Interfaces 2014, 6, 2700−2708

distance dependence of both one- and two-photon excitation fluorescence as observed in our studies.

In our current studies, local electric field amplification is expected to play a negligible role in OPEF of T790 because the one-photon excitation wavelength 420 nm is far off-resonance with the Plasmon modes of Au NRs, as confirmed by the FDTD simulation results shown in Figure 4. OPEF intensity

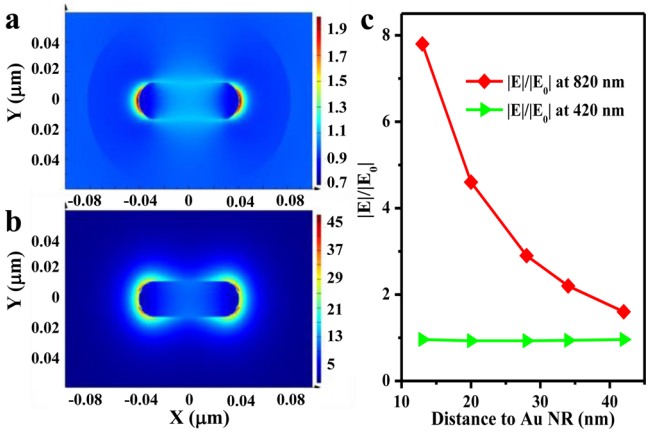

Figure 4. Simulated electric field (E) profile at (a) 420 nm and (b) 820 nm around an Au NR with longitudinal SPR band maximum at 820 nm. (c) Distance dependent electric field intensity along the longitudinal direction of Au NR. E_0 is electric field of incident light.

and quantum yield ($\phi = k_R/(k_R + k_{NR})$) are mainly determined by the interplay between enhanced radiative decay rates (k_R) and nonradiative energy transfer rate (k_{NR}), as plasmon resonance band of Au NRs has significant overlap with the emission spectrum of T790. At very large separation distances, the radiative decay rate will not be affected and energy transfer process does not occur. The emission efficiency will not be affected by the presence of metal nanoparticles for very large separation distances. This is consistent with our observation of enhancement factor of 1.1 at 42 nm, the largest shell thickness studied here. As the separation distance decreases, radiative decay rate starts to increase, fluorescence intensity and quantum yield (ϕ) increase, accompanied by shortening of fluorescence lifetime ($\tau = 1/(k_R + k_{NR})$). This is again consistent with our experimental observation when the shell thickness decreased from 42 to 34 nm. As the separation distance further decreases, both radiative decay and nonradiative energy transfer rates increase. However, the nonradiative energy transfer rate increases more rapidly and starts to takes a dominant role,[24,58] resulting in a decrease in both fluorescence quantum yield (ϕ) and lifetime (τ). Consequently, as the separation distance decreases, the overall OPEF intensity will first increase, reach the optimum enhancement and then become quenched again, while fluorescence lifetime will decrease steadily. This is well-consistent with our experimental observation (OPEF and lifetime data in Figure 3) and the theoretical predictions.[24,25]

Metal-enhanced TPEF is expected to follow a similar trend as OPEF. However, because of strong plasmon resonance of Au NRs at the excitation wavelength of 820 nm, local electric field amplification (Figure 4) will contribute additionally to enhance two-photon excitation efficiency and consequently enhance TPEF intensity. As two-photon excitation process involves absorption of two photons simultaneously, the excitation rate is proportional to the fourth power of local electric field.[31,59] The electric field amplification will decrease rapidly as the separation distance increases, as illustrated by the FDTD simulation results shown in Figure 4. Consequently the optimum TPEF is expected to occur at a shorter separation distance compared to OPEF. This is again well consistent with our experimental observation (Figure 3g). In our studies, enhanced TPEF of T790 in AuNR/SiO_2-T790 nanoparticles is due to the product of enhanced two-photon excitation efficiency and enhanced fluorescence quantum yield, while enhanced OPEF of T790 here is mainly due to enhanced quantum yield. The enhancement of two-photon excitation efficiency can thus be estimated by the ratio of TPEF enhancement factor over OPEF enhancement factor, as displayed in right axis of Figure 3g. Two-photon excitation efficiency was found to strongly depend on the silica shell thickness, with an optimum excitation enhancement factor of 32.8 at silica shell thickness of 20 nm. This result is consistent with a very recent report of maximum two-photon excitation enhancement of ~40 times.[23]

It is noted that TPEF enhancemnt of these core-shell nanoparticles is accompanied with shortened fluorescence lifetime. Enhanced TPEF renders them high efficiency for varous two-photon excitation based applications, while shortened fluorescence or excited state lifetime equips them with improved photostability. These features make them attractive in biological applications. Hematoporphyrin derivatives are photosensitizers widely used in photodynamic therapy (PDT) processes.[60] Two-photon photodynamic therapy has been known as a novel noninvasive cancer therapy method with many unique advantages compared to its one-photon counterpart, such as 3D localized treatment area, less side effect and deep penetration into biological tissues.[61−63] Effective photosensitizers for two-photon PDT require high singlet oxygen generation under two-photon excitation.[37,61] T790 is a widely investigated hematoporphyrin derivative with singlet oxygen generation yield of 0.47.[64] Its two-photon absorption cross section is quite small (~2 GM, see Table 1). In the presence of Au NRs, TPEF and two-photon excitation efficiency of T790 was found to be enhanced by factors of 11.8-fold and 32.8-fold, respectively, which is beneficial for their applications in two-photon photodynamic therapy.

Two-photon imaging capability of AuNR/SiO_2(20 nm)-T790 nanoparticles was demonstrated in HepG2 cancer cells (Figure 5), which can also be utilized to evaluate the uptake of AuNR/SiO_2-T790 nanoparticles by cancer cells. Two-photon imaging experiments were performed by using two-photon laser scanning confocal microscopy under femtosecond laser excitation at 820 nm and collecting emission signals from 600 to 650 nm. After incubation for 3 h, intense red emission

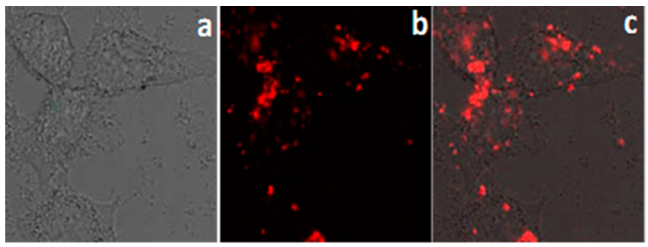

Figure 5. (a) Transmission image and (b) two-photon image of HepG2 cancer cells treated with AuNR/SiO_2(20 nm)-T790 nanoparticles. (c) Merged images. [AuNR/SiO_2-T790] = 40 pM. Scale bar is 20 μm.

dx.doi.org/10.1021/am405214w | ACS Appl. Mater. Interfaces 2014, 6, 2700−2708

signals were observed in the cytoplasm, indicating effective uptake of AuNR/SiO_2-T790 nanoparticles. This result confirms the capability of these AuNR/SiO_2(20 nm)-T790 nanoparticles to act as promising two-photon imaging agents. As the environment inside the cells is mainly aqueous, the observed two-photon emission mainly arises from TPPL of Au NRs (see Figure S1 in the Supporting Information).

A prerequisite for application of photosensitizers in PDT is high singlet oxygen generation efficiency. As biological applications are generally in aqueous media, singlet oxygen generation capability of these nanoparticles was evaluated in H_2O. The capability of singlet oxygen generation of AuNR/SiO_2-T790 under one- and two-photon excitation was evaluated by using a chemical method based on photo-oxidation of 9,10-anthracenediyl-bis(methylene) dimalonic acid (ABDA). In this approach, ABDA reacts with generated singlet oxygen to form an endoperoxide, resulting in a decrease in ABDA absorption band at 377 nm. Figure 6 shows photo-oxidation rate of ABDA

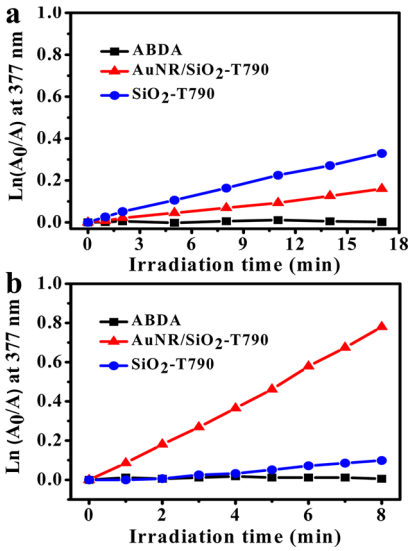

Figure 6. Photo-oxidation rates of ABDA in the presence of AuNR/SiO_2(20 nm)-T790 and SiO_2-T790 in H_2O under (a) one-photon excitation at 420 nm and (b) two-photon excitation at 800 nm. [AuNR/SiO_2-T790] = 40 pM.

in water in the presence of AuNR/SiO_2(20 nm)-T790 and SiO_2-T790 under one- and two-photon excitation. Under one-photon excitation at 420 nm, photo-oxidation rate of ABDA in the presence of AuNR/SiO_2(20 nm)-T790 was found to be ~0.49 times that of SiO_2-T790 with the same amount of T790. This is consistent with lower OPEF intensity of AuNR/SiO_2(20 nm)-T790 compared to SiO_2-T790. Reduced singlet oxygen generation capability can be ascribed to shortened excited state lifetime of T790. In contrast, photo-oxidation rate of ABDA in the presence of AuNR/SiO_2(20 nm)-T790 under two-photon excitation using femtosecond laser pulses at 800 nm is much faster (~7.9 time) than that in the presence of SiO_2-T790 (Figure 6b). This is again consistent with enhanced TPEF of AuNR/SiO_2(20 nm)-T790 compared to SiO_2-T790. Enhanced two-photon excitation efficiency of AuNR/SiO_2(20 nm)-T790 causes enhanced singlet oxygen generation while shortened excited state lifetime decreases singlet oxygen generation. The overall effect results in enhanced two-photon singlet oxygen generation. It needs to be noted that the above experiments were performed in H_2O solvent. Comparison of the results in DMF and H_2O solvents indicated that two-photon induced singlet oxygen generation capability of these AuNR/SiO_2-T790 nanoparticles in H_2O is significantly higher than that in DMF (see Figure S3 in the Supporting Information). This is because Au NR itself can generate singlet oxygen under two-photon excitation.[37] As singlet oxygen is the primary species responsible for PDT activity, these AuNR/SiO_2-T790 nanoparticles could thus be used as efficient photosensitizers in two-photon photodynamic therapy (TP-PDT).

Two-photon PDT activity of AuNR/SiO_2(20 nm)-T790 was evaluated on HepG2 cancer cells using the XTT assay (Figure 7). An unfocused femtosecond laser beam with a beam area of

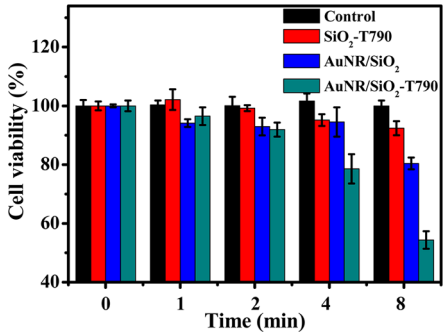

Figure 7. Time-dependent cell viability of HepG2 cancer cells after incubation with AuNR/SiO_2-T790 and SiO_2-T790 nanoparticles under femtosecond laser illumination at 800 nm (two-photon excitation). [AuNR/SiO_2-T790] = 40 pM, SiO_2-T790 has the same concentration of T790 as AuNR/SiO_2-T790. The control experiments without any nanoparticles were performed under the same irradiation conditions.

0.3 cm^2 and pulse energy of 0.9 mJ at 800 nm was used as the illumination source. These AuNR/SiO_2(20 nm)-T790 nanoparticles were found to display little dark cytotoxicity to cells for concentrations up to 100 pM (see Figure S4 in the Supporting Information). HepG2 cells incubated with AuNR/SiO_2(20 nm)-T790 (40 pM) were subjected to exposure of femtosecond laser illumination for different time periods. Cell viability was measured by colorimetric XTT metabolic activity assay after overnight incubation. The same experiments were performed on cells incubated with SiO_2-T790 and cells without incubation with any nanoparticles for direct comparison. The viability of cells without nanoparticles was almost 100% after laser irradiation for 8 min, suggesting that this dose of femtosecond laser irradiation power is safe for HepG2 cells. The viability of the cells treated with SiO_2-T790 under the same condition only showed a little bit killing effect: ~7% decrease in cell viability after laser irradiation for 8 min. In the presence of AuNR/SiO_2(20 nm), the viability of cells showed ~20% decrease after laser irradiation for 8 min. This is attributed to that Au NRs could also generate singlet oxygen under two-photon excitation.[48] In contrast, the viability of HepG2 cells treated with AuNR/SiO_2(20 nm)-T790 showed significant decrease as the irradiation time increases. Up to 50% of cancer cells were killed after femtosecond laser irradiation for 8 min. The significantly improved cancer cell killing efficiency is due to enhanced singlet oxygen generation of AuNR/SiO_2(20 nm)-T790 compared to SiO_2-T790 under two-photon excitation. These AuNR/SiO_2-T790 nanoparticles thus have great potential in acting as nano-photosensitizers in two-photon PDT.

CONCLUSIONS

In summary, AuNR/SiO_2-T790 core−shell nanoparticles with different silica shell thickness from 13 to 42 nm were prepared to systematically investigate gold nanorod enhanced one- and two-photon excitation fluorescence of T790. T790 molecules were covalently linked to the surface of silica coated Au NR by forming stable amide bonds. This conjugation method is a universal method for incorporating any fluorophores or biomolecules containing amine-reactive group onto silica shell. One- and two-photon excitation fluorescence intensities of T790 were found to strongly depend on the silica shell thickness that separates Au NR and T790. The optimum OPEF enhancement was found to occur at a shell thickness of 34 nm with an enhancement factor of 2.1, while the optimum TPEF enhancement was found to occur at 20 nm with a factor of 11.8. The fluorescence lifetime of T790 decreased steadily from 7.75 to 2.17 ns as the shell thickness decreased down to 13 nm. OPEF enhancement is attributed to the competition between increased radiative and non-radiative decay rates, while electric field amplification gives an additional contribution to TPEF enhancement. AuNR/SiO_2(20 nm)-T790, which displayed the largest TPEF enhancement, were also found to exhibit significantly improved singlet oxygen generation capability under two-photon excitation. The applications of these nanoparticles as effective agents for two-photon cell imaging and nano-photosensitizers for TP-PDT with improved efficiency have been demonstrated on HepG2 cancer cells using the XTT assay. The remarkable two-photon excitation fluorescence enhancement property of these AuNR/SiO_2-T790 nanoparticles makes them promising agents for two-photon imaging guided two-photon phototherapy.

ASSOCIATED CONTENT

Supporting Information

TEM image, optical properties of SiO_2-T790; optical properties of AuNR/SiO_2(28 nm)-T790 in DMF/H_2O mixed solvents; comparison of two-photon singlet oxygen generation of AuNR/SiO_2(28 nm)-T790 in DMF and H_2O solvents; cytotoxicity of AuNR/SiO_2(20 nm)-T790 in HepG2 cells. This material is available free of charge via the Internet at http://pubs.acs.org.

AUTHOR INFORMATION

Corresponding Authors

*E-mail: chmxqh@nus.edu.sg. Fax: +65 6779-1691. Tel: +65 6516-2847 (X.Q.H.).

*E-mail: chmxugq@nus.edu.sg (X.G.Q.).

Author Contributions

†Authors T.Z. and K.Y. contributed equally to this work.

Notes

The authors declare no competing financial interest.

ACKNOWLEDGMENTS

We thank the financial support from DSTA Singapore (Project DSTA-NUS-DIRP/9010100347) and Competitive Research program under Singapore National Research Foundation (NRF-CRP10-2012-04).

REFERENCES

(1) Kelly, K. L.; Coronado, E.; Zhao, L. L.; Schatz, G. C. *J. Phys. Chem. B* **2003**, *107*, 668−677.

(2) Murphy, C. J.; San, T. K.; Gole, A. M.; Orendorff, C. J.; Gao, J. X.; Gou, L.; Hunyadi, S. E.; Li, T. *J. Phys. Chem. B* **2005**, *109*, 13857−13870.

(3) Tian, Z. Q.; Ren, B.; Li, J. F.; Yang, Z. L. *Chem. Commun.* **2007**, 3514−3534.

(4) Willets, K. A.; Van Duyne, R. P. *Annu. Rev. Phys. Chem.* **2007**, *58*, 267−297.

(5) Lakowicz, J. R. *Anal. Biochem.* **2001**, *298*, 1−24.

(6) Lakowicz, J. R. *Anal. Biochem.* **2005**, *337*, 171−194.

(7) Sapsford, K. E.; Berti, L.; Medintz, I. L. *Angew. Chem., Int. Ed.* **2006**, *45*, 4562−4588.

(8) Aslan, K.; Geddes, C. D. *Chem. Soc. Rev.* **2009**, *38*, 2556−2564.

(9) Geddes, C. D.; Lakowicz, J. R. *J. Fluoresc.* **2002**, *12*, 121−129.

(10) Guan, Z. P.; Polavarapu, L.; Xu, Q. H. *Langmuir* **2010**, *26*, 18020−18023.

(11) Polavarapu, L.; Mamidala, V.; Guan, Z. P.; Ji, W.; Xu, Q. H. *Appl. Phys. Lett.* **2012**, *100*, 023106.

(12) Bouhelier, A.; Beversluis, M.; Hartschuh, A.; Novotny, L. *Phys. Rev. Lett.* **2003**, *90*, 013903.

(13) Cheng, D.; Xu, Q.-H. *Chem. Commun.* **2007**, 248−250.

(14) Tovmachenko, O. G.; Graf, C.; van den Heuvel, D. J.; van Blaaderen, A.; Gerritsen, H. C. *Adv. Mater.* **2006**, *18*, 91−95.

(15) Aslan, K.; Wu, M.; Lakowicz, J. R.; Geddes, C. D. *J. Am. Chem. Soc.* **2007**, *129*, 1524−1525.

(16) Zhang, J.; Fu, Y.; Chowdhury, M. H.; Lakowicz, J. R. *Nano Lett.* **2007**, *7*, 2101−2107.

(17) Pompa, P. P.; Martiradonna, L.; Della Torre, A.; Della Sala, F.; Manna, L.; De Vittorio, M.; Calabi, F.; Cingolani, R.; Rinaldi, R. *Nat. Nanotechnol.* **2006**, *1*, 126−130.

(18) Kano, H.; Kawata, S. *Opt. Lett.* **1996**, *21*, 1848−1850.

(19) Wenseleers, W.; Stellacci, F.; Meyer-Friedrichsen, T.; Mangel, T.; Bauer, C. A.; Pond, S. J. K.; Marder, S. R.; Perry, J. W. *J. Phys. Chem. B* **2002**, *106*, 6853−6863.

(20) Jung, J. M.; Yoo, H. W.; Stellacci, F.; Jung, H. T. *Adv. Mater.* **2010**, *22*, 2542−2546.

(21) Zhang, Y. N.; Birch, D. J. S.; Chen, Y. *Appl. Phys. Lett.* **2011**, *99*, 103701.

(22) Cohanoschi, I.; Yao, S.; Belfield, K. D.; Hernandez, F. E. *J. Appl. Phys.* **2007**, *101*, 086112.

(23) Sivapalan, S. T.; Vella, J. H.; Yang, T. K.; Dalton, M. J.; Swiger, R. N.; Haley, J. E.; Cooper, T. M.; Urbas, A. M.; Tan, L.-S.; Murphy, C. J. *Langmuir* **2012**, *28*, 9147−9154.

(24) Bharadwaj, P.; Novotny, L. *Opt. Express* **2007**, *15*, 14266−14274.

(25) Anger, P.; Bharadwaj, P.; Novotny, L. *Phys. Rev. Lett.* **2006**, *96*, 113002.

(26) Yuan, P. Y.; Lee, Y. H.; Gnanasammandhan, M. K.; Guan, Z. P.; Zhang, Y.; Xu, Q. H. *Nanoscale* **2012**, *4*, 5132−5137.

(27) Zijlstra, P.; Chon, J. W. M.; Gu, M. *Nature* **2009**, *459*, 410−413.

(28) Li, C. Z.; Male, K. B.; Hrapovic, S.; Luong, J. H. T. *Chem. Commun.* **2005**, 3924−3926.

(29) Oyelere, A. K.; Chen, P. C.; Huang, X. H.; El-Sayed, I. H.; El-Sayed, M. A. *Bioconjugate Chem.* **2007**, *18*, 1490−1497.

(30) Yu, C. X.; Irudayaraj, J. *Anal. Chem.* **2007**, *79*, 572−579.

(31) Wang, H. F.; Huff, T. B.; Zweifel, D. A.; He, W.; Low, P. S.; Wei, A.; Cheng, J. X. *Proc. Natl. Acad. Sci. U.S.A.* **2005**, *102*, 15752−15756.

(32) Durr, N. J.; Larson, T.; Smith, D. K.; Korgel, B. A.; Sokolov, K.; Ben-Yakar, A. *Nano Lett.* **2007**, *7*, 941−945.

(33) Chen, C. C.; Lin, Y. P.; Wang, C. W.; Tzeng, H. C.; Wu, C. H.; Chen, Y. C.; Chen, C. P.; Chen, L. C.; Wu, Y. C. *J. Am. Chem. Soc.* **2006**, *128*, 3709−3715.

(34) Wei, Q. S.; Ji, J.; Shen, J. C. *Macromol. Rapid Commun.* **2008**, *29*, 645−650.

(35) Huang, X. H.; El-Sayed, I. H.; Qian, W.; El-Sayed, M. A. *J. Am. Chem. Soc.* **2006**, *128*, 2115−2120.

(36) Dickerson, E. B.; Dreaden, E. C.; Huang, X. H.; El-Sayed, I. H.; Chu, H. H.; Pushpanketh, S.; McDonald, J. F.; El-Sayed, M. A. *Cancer Lett.* **2008**, *269*, 57−66.

(37) Zhao, T. T.; Shen, X. Q.; Li, L.; Guan, Z. P.; Gao, N. Y.; Yuan, P. Y.; Yao, S. Q.; Xu, Q.-H.; Xu, G. Q. *Nanoscale* **2012**, *4*, 7712−7719.
(38) Ming, T.; Zhao, L.; Yang, Z.; Chen, H.; Sun, L.; Wang, J.; Yan, C. *Nano Lett.* **2009**, *9*, 3896−3903.
(39) Zhao, L.; Ming, T.; Chen, H. J.; Liang, Y.; Wang, J. F. *Nanoscale* **2011**, *3*, 3849−3859.
(40) Bardhan, R.; Grady, N. K.; Cole, J. R.; Joshi, A.; Halas, N. J. *ACS Nano* **2009**, *3*, 744−752.
(41) Gabudean, A. M.; Focsan, M.; Astilean, S. *J. Phys. Chem. C* **2012**, *116*, 12240−12249.
(42) Yang, Z.; Ni, W. H.; Kou, X. S.; Zhang, S. Z.; Sun, Z. H.; Sun, L. D.; Wang, J. F.; Yan, C. H. *J. Phys. Chem. C* **2008**, *112*, 18895−18903.
(43) Nikoobakht, B.; El-Sayed, M. A. *Chem. Mater.* **2003**, *15*, 1957−1962.
(44) Jana, N. R.; Gearheart, L.; Murphy, C. J. *J. Phys. Chem. B* **2001**, *105*, 4065−4067.
(45) Gou, L. F.; Murphy, C. J. *Chem. Mater.* **2005**, *17*, 3668−3672.
(46) Stober, W.; Fink, A.; Bohn, E. *J. Colloid Interface Sci.* **1968**, *26*, 62−69.
(47) Johnson, P. B.; Christy, R. W. *Phys. Rev. B* **1972**, *6*, 4370−4379.
(48) Zhao, T. T.; Wu, H.; Yao, S. Q.; Xu, Q. H.; Xu, G. Q. *Langmuir* **2010**, *26*, 14937−14942.
(49) Pastoriza-Santos, I.; Perez-Juste, J.; Liz-Marzan, L. M. *Chem. Mater.* **2006**, *18*, 2465−2467.
(50) Jiang, K. Y.; Schadler, L. S.; Siegel, R. W.; Zhang, X. J.; Zhang, H. F.; Terrones, M. *J. Mater. Chem.* **2004**, *14*, 37−39.
(51) Zeeman, R.; Dijkstra, P. J.; van Wachem, P. B.; van Luyn, M. J. A.; Hendriks, M.; Cahalan, P. T.; Feijen, J. *Biomaterials* **1999**, *20*, 921−931.
(52) Lessard-Viger, M.; Rioux, M.; Rainville, L.; Boudreau, D. *Nano Lett.* **2009**, *9*, 3066−3071.
(53) Mohamed, M. B.; Volkov, V.; Link, S.; El-Sayed, M. A. *Chem. Phys. Lett.* **2000**, *317*, 517−523.
(54) Zhao, T.; Jiang, X.-F.; Gao, N.; Li, S.; Zhou, N.; Ma, R.; Xu, Q.-H. *J. Phys. Chem. B* **2013**, *117*, 15576−15583.
(55) Finikova, O. S.; Troxler, T.; Senes, A.; DeGrado, W. F.; Hochstrasser, R. M.; Vinogradov, S. A. *J. Phys. Chem. A* **2007**, *111*, 6977−6990.
(56) Brinas, R. P.; Troxler, T.; Hochstrasser, R. M.; Vinogradov, S. A. *J. Am. Chem. Soc.* **2005**, *127*, 11851−11862.
(57) Orendorff, C. J.; Murphy, C. J. *J. Phys. Chem. B* **2006**, *110*, 3990−3994.
(58) Lakowicz, J. R. *Anal. Biochem.* **2001**, *298*, 1−24.
(59) Gryczynski, I.; Malicka, J.; Shen, Y. B.; Gryczynski, Z.; Lakowicz, J. R. *J. Phys. Chem. B* **2002**, *106*, 2191−2195.
(60) Fiel, R. J.; Dattagupta, N.; Mark, E. H.; Howard, J. C. *Cancer Res.* **1981**, *41*, 3543−3545.
(61) Velusamy, M.; Shen, J. Y.; Lin, J. T.; Lin, Y. C.; Hsieh, C. C.; Lai, C. H.; Lai, C. W.; Ho, M. L.; Chen, Y. C.; Chou, P. T.; Hsiao, J. K. *Adv. Funct. Mater.* **2009**, *19*, 2388−2397.
(62) Kim, S.; Ohulchanskyy, T. Y.; Pudavar, H. E.; Pandey, R. K.; Prasad, P. N. *J. Am. Chem. Soc.* **2007**, *129*, 2669−2675.
(63) Frederiksen, P. K.; Jorgensen, M.; Ogilby, P. R. *J. Am. Chem. Soc.* **2001**, *123*, 1215−1221.
(64) Gerdes, R.; Wohrle, D.; Spiller, W.; Schneider, G.; Schnurpfeil, G.; Schulz-Ekloff, G. *J. Photochem. Photobiol. A* **1997**, *111*, 65−74.